1-1-2017

# Enhancing Light Transmission through a Disordered Waveguide with Inhomogeneous Scattering and Loss

Raktim Sarma

Alexey Yamilov
*Missouri University of Science and Technology*, yamilov@mst.edu

Hui Cao



## Recommended Citation

R. Sarma et al., "Enhancing Light Transmission through a Disordered Waveguide with Inhomogeneous Scattering and Loss," *Applied Physics Letters*, vol. 110, no. 2, pp. 021103-1-021103-4, American Institute of Physics (AIP), Jan 2017.
The definitive version is available at https://doi.org/10.1063/1.4973459

# Enhancing light transmission through a disordered waveguide with inhomogeneous scattering and loss

Raktim Sarma,[1] Alexey Yamilov,[2,a)] and Hui Cao[1,b)]
[1]Department of Applied Physics, Yale University, New Haven, Connecticut 06520, USA
[2]Department of Physics, Missouri University of Science and Technology, Rolla, Missouri 65409, USA

(Received 16 October 2016; accepted 11 December 2016; published online 9 January 2017)

We enhanced the total transmission of light through a disordered waveguide with spatially inhomogeneous scattering and loss by shaping the incident wavefront of a laser beam. Using an on-chip tapered lead, we were able to access all input modes in the waveguide with a spatial light modulator. The adaptive wavefront shaping resulted in selective coupling of input light to high transmission channels, which bypassed the regions of higher scattering and loss in the waveguide. Spatial inhomogeneity in scattering and loss leads to the modification of the spatial structures of transmission eigenchannels, allowing wavefront shaping to redirect the energy flux to circumvent regions of higher scattering and loss and thereby enhancing the energy transported through the system. This work demonstrates the power of wavefront shaping in coherent control of light transport in inhomogeneous scattering media, which are common in real applications. *Published by AIP Publishing.* [http://dx.doi.org/10.1063/1.4973459]

In the recent years, there have been rapid advances in coherent control of light propagation in strong scattering media.[1] It has been shown that light can be focused inside or through a turbid medium by shaping the input wavefront,[2] which enables image transmission through an opaque material.[3] Wavefront shaping techniques have also been used to enhance the total transmission of light through a diffusive scattering system via selective coupling of incident light to high transmission channels.[4–9] These studies have important implications in biophotonics and biomedical applications.[10,11] However, in real scattering samples such as biological tissues, the amount of light scattering often varies spatially. So far, all the lossless diffusive samples used in wavefront shaping experiments are homogeneous, namely, the scattering strength that is constant everywhere. Coherent control of light transport has not been demonstrated in samples with inhomogeneous scattering, and the power of wavefront shaping in such systems is not known.

Light absorption is common in optical systems, and it can strongly modify high transmission channels. With strong absorption uniformly spread across a diffusive scattering medium, the diffusive transport of light in the maximum transmission channel turns into quasi-ballistic.[12] In reality, optical absorbers are often distributed non-uniformly in random samples. Wavefront shaping technique has been used to force light to go around local absorbers inserted in between two glass diffusers.[13] The scattering is relatively weak in this experiment. In a diffusive system with much stronger scattering, it has been shown numerically that the high transmission channels redirect the energy flow to circumvent the absorbing regions to minimize attenuation.[14] These results for a diffusive system are obtained from numerical simulations, and there has been no experimental study yet. Although experimentally, bypassing of regions of higher absorption by light has been demonstrated in a system where a painted cover was inserted between two glass diffusers,[13] the transport through that system in a single iteration was quasi-ballistic and not completely diffusive. Furthermore, it is neither clear nor has it been shown what will happen when both scattering and absorption are spatially inhomogeneous.

In this paper, we adopt the adaptive wavefront shaping approach to enhance light transmission through a disordered waveguide with spatially inhomogeneous scattering and loss. Unlike the previous works of using wavefront shaping to guide light through multimode fibers,[15–21] light in the disordered waveguide experiences strong backscattering. More specifically, we fabricate a silicon waveguide that contains randomly distributed air holes within photonic crystal sidewalls. The degree of input control is much higher than that in the open slab geometry, thanks to an on-chip tapered lead. Light transport inside the two dimensional disordered waveguide can be directly probed from the third dimension. After optimizing the input wavefront to enhance the total transmission, we observe that optical waves bypass the region of higher scattering and loss in the waveguide. The spatial inhomogeneity of scattering and loss leads to redirecting of energy flux to optical paths with less scattering and loss, in order to maximize the total energy transported through the system. The experimental data agree to the numerical simulation results, revealing how a high transmission channel is modified by spatially inhomogeneous scattering and loss.

The disordered waveguide was fabricated in a silicon-on-insulator (SOI) wafer. The thicknesses of the silicon layer and of the buried oxide were 220 nm and 3 $\mu$m, respectively. The patterns were made by electron beam lithography and etched by an inductively coupled-plasma (ICP) reactive-ion-etcher (RIE). Figure 1 is the scanning electron microscope (SEM) image of a fabricated sample. The waveguide is $L = 60\,\mu$m long and $W = 20\,\mu$m wide. It contained a two-dimensional (2D) random array of air holes. While propagating in the waveguide, light is scattered both in plane and out

a)Electronic mail: yamilov@mst.edu
b)Electronic mail: hui.cao@yale.edu

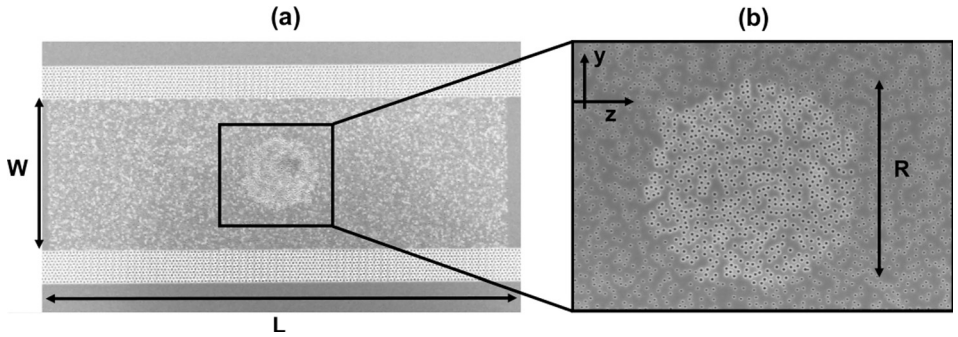


FIG. 1. 2D disordered waveguide with inhomogeneous scattering and loss. (a) Top-view scanning electron micrograph (SEM) of the fabricated silicon waveguide that consists of randomly positioned air holes. The waveguide width $W = 20\,\mu$m and length $L = 60\,\mu$m. A circular region of diameter $R = 10\,\mu$m at the center of the waveguide has larger and denser air holes (hole diameter = 150 nm, the air filling fraction = 15%). Outside this region, the air holes are smaller (diameter = 90 nm) and the filling fraction is lower (6%). The sidewalls of the waveguide are made of a triangular lattice of air holes (diameter = 360 nm, lattice constant = 505 nm), which supports an in-plane photonic bandgap at the wavelength $\lambda = 1.51\,\mu$m. (b) Magnified SEM of the central region of the disordered waveguide showing air holes of two different sizes and densities. The light propagates in the $z$ direction.

of plane by the air holes. The out-of-plane scattering can be treated as loss, and the material absorption at the probe wavelength ($\lambda = 1510$ nm) is negligible.[22]

To introduce spatially inhomogeneous scattering and loss, we varied the size and density of air holes in the waveguide. In a central region of diameter $R = 10\,\mu$m, the air holes are larger and denser (hole diameter = 150 nm, air filling fraction = 15%), leading to stronger in-plane scattering and out-of-plane scattering. Outside this region, the scattering and loss are weaker, as the air holes are smaller (diameter = 90 nm) and the filling fraction is lower (6%).

The relevant parameters to describe light propagation in the disordered waveguide are the transport mean free path $\ell$ and the diffusive dissipation length $\xi_a$. Their values in the two regions of different air hole size and density were extracted from the measurement of intensity distributions and fluctuations in two separate waveguides with homogeneous scattering and loss.[23] In the central region, $\ell = 1\,\mu$m and $\xi_a = 13\,\mu$m; in the surrounding region, $\ell = 2.5\,\mu$m and $\xi_a = 31\,\mu$m.

The waveguide had reflecting sidewalls made of a triangular lattice of air holes (diameter = 360 nm, lattice constant = 550 nm). It supported an in-plane photonic bandgap at the probe wavelength that confined the scattered light within the waveguide. The incident light was injected from the edge of the wafer to a silicon ridge waveguide. Due to the refractive index mismatch between silicon and air, the light could only excite the lower-order modes of the ridge waveguide, limiting the number of input modes that could be controlled by wavefront shaping. To increase the degree of input control, we designed and fabricated a tapered waveguide that served as a lead to the disordered waveguide.[9] The tapering angle was 15°, and the waveguide width was reduced from 330 $\mu$m to 20 $\mu$m over a length of 578 $\mu$m. The wider waveguide at the input supported many more lower-order modes that were converted into higher-order modes by the taper. The numerical simulation confirmed that the number of waveguide modes excited at the air-silicon interface by the incident light is significantly larger than the number of transmission channels in the disordered waveguide $N = 75$.

To control light transport in the disordered waveguide, we adopted the adaptive wavefront shaping scheme that we had recently implemented for 2D on-chip waveguides.[9] The setup is shown schematically in Fig. 2. A monochromatic laser beam was collimated, expanded and linearly polarized. It is then phase modulated by a spatial light modulator (SLM). The SLM plane was demagnified by about a factor of 3 and projected to the pupil plane of an objective. At the

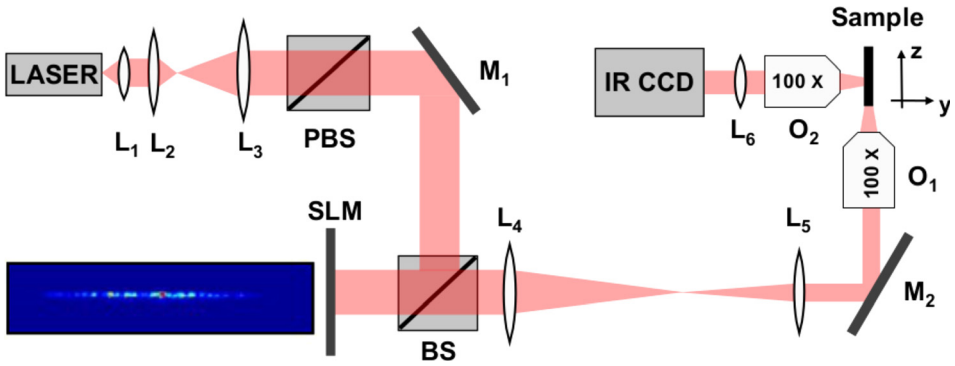


FIG. 2. A schematic of the wavefront shaping experiment setup. A laser beam (HP 8168F) at $\lambda = 1510$ nm is collimated (by lens $L_1$), expanded (by $L_2$, $L_3$), and linearly polarized (by a polarized beam splitter PBS) before being modulated by a phase-only SLM (Hamamatsu X10468). Two lens ($L_4$, $L_5$) are used to project the SLM plane to the pupil plane of an objective $O_1$ (100×, NA = 0.7), and the edge of the coupling waveguide is placed at the focal plane of the objective. The light scattered out of the sample plane is collected by a second objective $O_2$ (100×, NA = 0.7) and imaged to an InGaAs camera (Xenics XEVA 1.7–320) by a tube lens ($L_6$). $M_1$ and $M_2$ are mirrors; BS is an unpolarized beam splitter. The inset is an optical image of the illumination line on the front facet of the coupling waveguide, created by modulating the phase of the SLM pixels.

focal plane of objective lied the front facet of the coupling waveguide. We imposed one-dimensional phase modulation on the SLM to create a line of illumination for the coupling waveguide, as shown in the inset of Fig. 2. The front end of the coupling waveguide is 330 $\mu$m wide and supports 1245 guided modes in total. Due to the large index mismatch at the silicon/air interface and the finite numerical aperture of the objective lens, the incident light is coupled to 359 lower order modes, which are then converted into higher order modes by the taper. The number of macropixels of the SLM that we controlled was 300, exceeding the number of modes in the disordered waveguide (75), in average the number of SLM macropixels per mode was 4. To map the spatial distribution of light intensity, $I(y, z)$, inside the disordered structure, the out-of-plane scattered light was collected by a second objective and projected to an InGaAs camera.

To enhance the total transmission through the disordered waveguide, we chose the feedback-based optimization technique, which was robust against the measurement noise. The cost function $S$ was given by the ratio of the cross-section integrated intensity of light at the back end of the waveguide over that at the front end. Note that $S$ was not equal to the total transmission, as the intensity at the front end included both incident and reflected light. To smooth out the fluctuation, the intensity was integrated over an area of length $d = 12.5\ \mu$m and width $W = 20\ \mu$m. We used the continuous sequential algorithm to maximize $S$ by adjusting the phase of SLM pixels.[2] To ensure the convergence of the optimization algorithm, the phases of all 300 macro-pixels were adjusted in two sequential rounds and the iteration process took approximately 15 min that was limited by the speed of the InGaAs camera. Figures 3(a) and 3(b) show the intensity distribution $I(y, z)$ for an un-optimized input (produced by assigning random phases to the SLM macropixels) and an optimized input, respectively. When the input wavefront was not optimized, the light intensity decreased with the depth in the disordered waveguide. Stronger out-of-plane scattering brightened the central region that had larger and denser air holes. In contrast, the optimized input wavefront (corresponding to an increase in $S$ by 78%) made the central region dark, while the intensities on both sides of this region

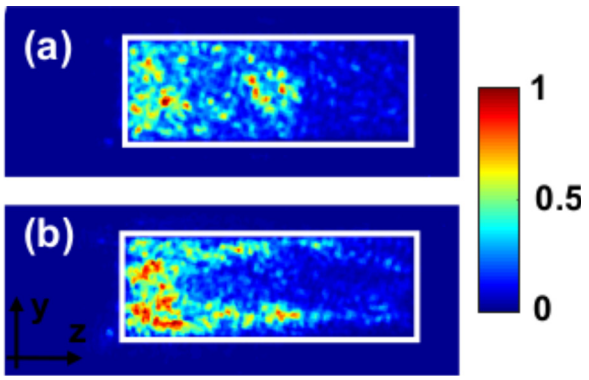


FIG. 3. Optimizing the incident wavefront to enhance light transmission through the disordered waveguide with spatially inhomogeneous scattering and loss. Experimentally measured 2D intensity distribution $I(y, z)$ inside the waveguide shown in Fig. 1 for (a) unoptimized input fields and (b) optimized input for maximum cost function $S$. The white box marks the boundary of the disordered waveguide.

increased. Such changes indicated that light bypassed the central region with higher scattering and loss to maximize the total energy transported through the medium.

For a better understanding of the experimental results, in order to understand the energy flow for optimized input, we performed a numerical simulation[24] to calculate the ensemble averaged Poynting vector $\vec{J}(y, z)$ for an optimized input of a 2D disordered waveguide with all parameters equal to the experimental values. The continuous sequential algorithm was used to optimize the total transmission via phase-only modulation of the input wavefront. The total transmission was increased from 3.2% with an unoptimized input to 42% with an optimized input. As long as we control all input modes of the disordered waveguide, the improvement in transmission is independent of the setup parameters but instead depends on the sample parameters such as the strength of scattering and loss, the waveguide dimension, and the inhomogeneity.

Figure 4(a) plots the magnitude and direction of $\vec{J}(y, z)$ in the disordered waveguide for an optimized input. The optimized input wavefront made the energy flux circumvent the central region with higher scattering and loss, in agreement with the experimental result. Most light bypassed the central region with stronger scattering and loss by transmitting through top or bottom region, leading to an increase in the local intensity. After passing the central region, both scattering and dissipation become uniform across the waveguide, and light spreads in the transverse direction, resulting in a rapid reduction in the density. The remaining loss outside the central region causes a further decay of light intensity.

Fig. 4(b) shows the magnitude and direction of $\vec{J}(y, z)$ of the maximum transmission channel, which resembles that of the optimized input in Fig. 4(a). The correlation between Figs. 4(a) and 4(b) is 0.99. This result suggested that with the optimized input wavefront, light transport was dominated by the maximum transmission channel. This was further confirmed by decomposing the optimized input wavefront by the transmission eigenchannels, and the contribution from the maximum transmission channel was found to be significantly

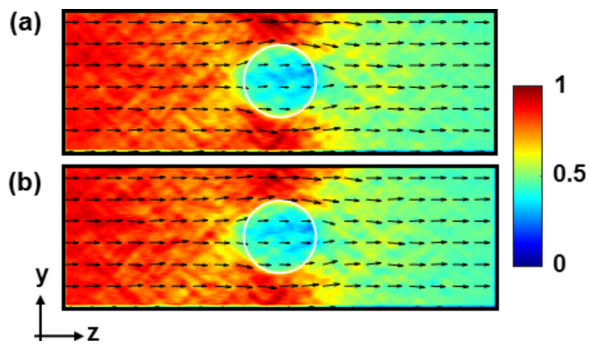


FIG. 4. Numerical simulation of the ensemble averaged Poynting vector $\vec{J}(y, z)$ of light inside the 2D disordered waveguide with spatially inhomogeneous scattering and loss. The magnitude of $\vec{J}(y, z)$ is shown by color plot, and its direction is shown by the arrows. The input field in (a) is optimized to maximize total transmission. With optimized input wavefront, the optical waves bypass the region of higher scattering and loss in the middle of the waveguide (denoted by a while circle). (b) shows $\vec{J}(y, z)$ for the maximum transmission channel, which is nearly identical to that in (a), indicating the optimized input field couples mostly to the maximum transmission channel.

larger than all other channels. Therefore, the optimization of incident wavefront led to selective coupling of light to the high transmission channels.

In summary, we enhanced light transmission through a 2D waveguide with spatially inhomogeneous scattering and loss by shaping the wavefront of incident light. Using a tapered lead, we were able to access all input modes by a spatial light modulator. The optimized wavefront selectively coupled light to high transmission channels, which bypass the regions of higher scattering and loss. This work demonstrated the power of wavefront shaping in controlling light transport in inhomogeneous scattering samples, which are common in real applications. In addition, our results may trigger further studies of on-chip disordered photonic nanostructures with spatially varying scattering strength and loss to mold the flow of light.[25]

We acknowledge Chia-Wei Hsu, Douglas Stone, Hasan Yilmaz, and Seng Fatt Liew for the useful discussions. This work was supported by the Office of Naval Research (ONR) under Grant No. MURI N00014-13-0649, by the US-Israel Binational Science Foundation (BSF) under Grant No. 2015509 and by the National Science Foundation (NSF) under Grant No. NSF DMR-1205223. Facilities use was supported by YINQE and NSF MRSEC DMR-1119826.

[1]A. P. Mosk, A. Lagendijk, G. Lerosey, and M. Fink, Nat. Photonics **6**, 283 (2012).
[2]I. M. Vellekoop, Opt. Express **23**, 12189 (2015).
[3]S. Popoff, G. Lerosey, M. Fink, A. C. Boccara, and S. Gigan, Nat. Commun. **1**, 81 (2010).
[4]I. M. Vellekoop and A. P. Mosk, Phys. Rev. Lett. **101**, 120601 (2008).
[5]W. Choi, A. P. Mosk, Q. H. Park, and W. Choi, Phys. Rev. B **83**, 134207 (2011).
[6]M. Kim, Y. Choi, C. Yoon, W. Choi, J. Kim, Q.-H. Park, and W. Choi, Nat. Photonics **6**, 581 (2012).
[7]H. Yu, T. R. Hillman, W. Choi, J. O. Lee, M. S. Feld, R. R. Dasari, and Y. K. Park, Phys. Rev. Lett. **111**, 153902 (2013).
[8]S. M. Popoff, A. Goetschy, S. F. Liew, A. D. Stone, and H. Cao, Phys. Rev. Lett. **112**, 133903 (2014).
[9]R. Sarma, A. Yamilov, S. Petrenko, Y. Bromberg, and H. Cao, Phys. Rev. Lett. **117**, 086803 (2016).
[10]M. Kim, W. Choi, Y. Choi, C. Yoon, and W. Choi, Opt. Express **23**, 12648 (2015).
[11]H. Yu, J. Park, K. Lee, J. Yoon, K. Kim, S. Lee, and Y. Park, Curr. Appl. Phys. **15**, 632 (2015).
[12]S. F. Liew, S. M. Popoff, A. P. Mosk, W. L. Vos, and H. Cao, Phys. Rev. B **89**, 224202 (2014).
[13]X. Hao, L. Martin-Rouault, and M. Cui, Sci. Rep. **4**, 5874 (2014).
[14]S. F. Liew and H. Cao, Opt. Express **23**, 11043 (2015).
[15]T. Čižmár and K. Dholakia, Nat. Commun. **3**, 1027 (2012).
[16]Y. Choi, C. Yoon, M. Kim, T. D. Yang, C. Fang-Yen, R. R. Dasari, K. J. Lee, and W. Choi, Phys. Rev. Lett. **109**, 203901 (2012).
[17]A. M. Caravaca-Aguirre, E. Niv, D. B. Conkey, and R. Piestun, Opt. Express **21**, 12881 (2013).
[18]R. Y. Gu, R. N. Mahalati, and J. M. Kahn, Opt. Express **23**, 26905 (2015).
[19]J. Carpenter, B. J. Eggleton, and J. Schröder, Nat. Photonics **9**, 751 (2015).
[20]J. W. Czarske, D. Haufe, N. Koukourakis, and L. Büttner, Opt. Express **24**, 15128 (2016).
[21]W. Xiong, P. Ambichl, Y. Bromberg, B. Redding, S. Rotter, and H. Cao, Phys. Rev. Lett. **117**, 053901 (2016).
[22]A. Yamilov, R. Sarma, B. Redding, B. Payne, H. Noh, and H. Cao, Phys. Rev. Lett. **112**, 023904 (2014).
[23]R. Sarma, A. Yamilov, P. Neupane, and H. Cao, Phys. Rev. B **92**, 180203 (2015).
[24]C. W. Groth, M. Wimmer, A. R. Akhmerov, and X. Waintal, New J. Phys. **16**, 063065 (2014).
[25]M. Koirala and A. Yamilov, Opt. Lett. **41**, 3860 (2016).